

Evaluation of Temperature Distribution in the Tuner of the FNAL Booster's Tunable Second Harmonic Cavity

I. Terechkine and G. Romanov

A second harmonic cavity of Fermilab's Booster must generate 100 kV accelerating voltage and be tunable in the frequency range from 75 to 105 MHz during the 33 ms accelerating cycle with 15 Hz repetition rate. Among other factors, feasibility of this device depends on the ability to restrict the temperature growth in the ferrite material of the tuner. In accordance to [1], RF loss power density in the ferrite strongly depends on the internal magnetic field, which practically is never uniform in the material; moreover, in some areas of the tuner, the field is in a high degree of non-uniformity, and so is the RF loss power density. On the other hand, internal magnetic field is a function of static permeability of the material, which strongly depends on the magnetic field and is also a function of the temperature. That's why, to ensure that the temperature inside the tuner is acceptable, for every version of the design, thermal analysis must be made. A way to make this kind of a study was suggested in [2]. This note summarizes results of the studies for the latest version of the cavity design; some modifications to suggested in [2] method of the analysis were used here that simplify the analysis in the areas of the tuner where bias magnetic field is not severely non-uniform.

Geometry of the cavity is shown in Fig. 1.

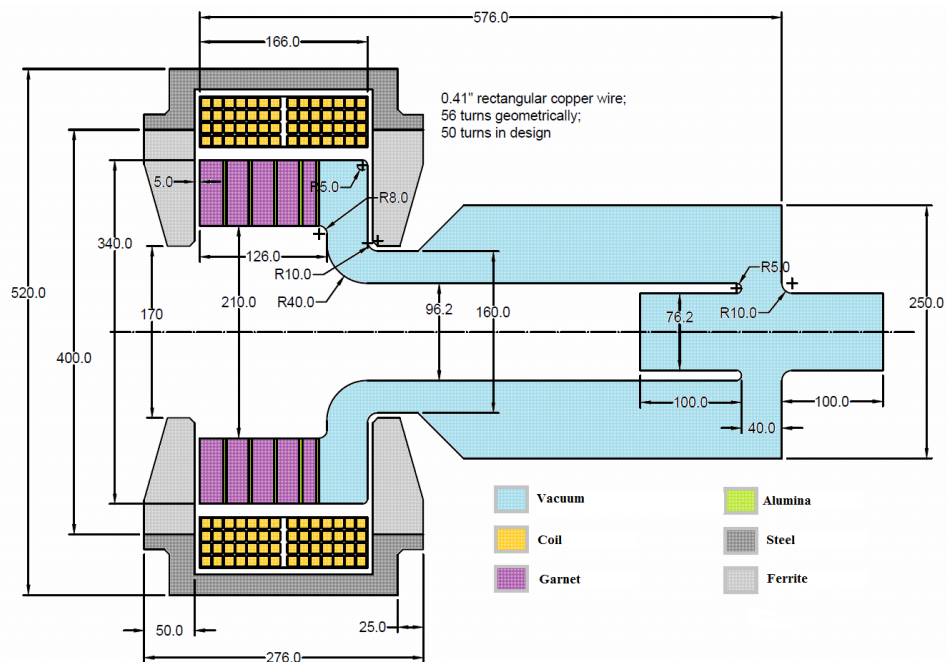


Fig. 1. 2D version of the RF design of the FNAL Booster's 2-nd harmonic cavity.

The tuner of the cavity is subdivided into several sections (blocks) separated by thin discs made of alumina, which were introduced to facilitate the heat removal. Thicknesses of the blocks differ: starting from the tuner end of the cavity, they are 23.5 mm, 22 mm, 22 mm, 22 mm, and 13.5 mm. Thickness of each alumina disk is 3 mm.

The bias coil is wound using 0.41" rectangular copper wire with a 0.2" diameter channel for water cooling; the number of turns in the coil is 50. The flux return must allow operation at frequencies up to ~50 Hz, so it must be made using solid ferrite pieces and/or laminated silicon steel blocks.

In the Booster beam line, during each 33 ms accelerating cycle, the cavity must deliver 100 kV accelerating voltage within two three-millisecond periods. Time diagram in Fig. 2 shows frequency change during one acceleration cycle and the timing of the accelerating voltage.

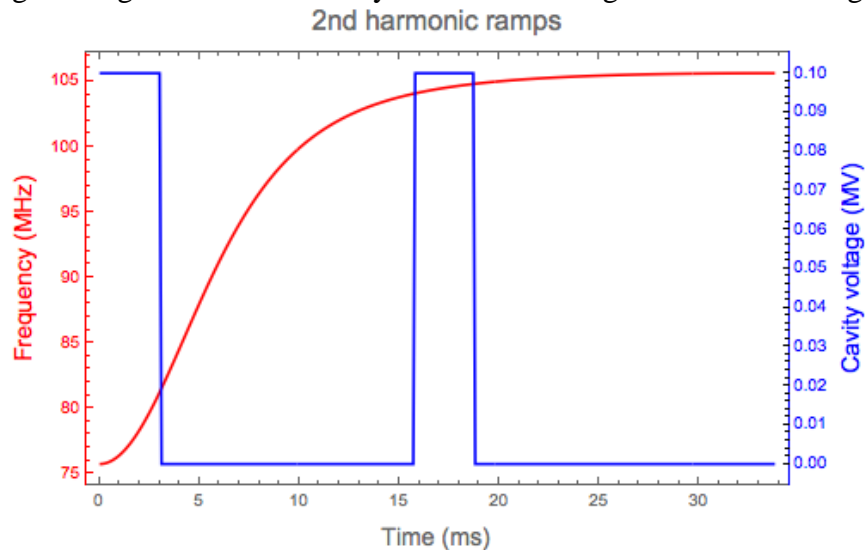


Fig. 2. Frequency ramp and the accelerating voltage in the 2-nd harmonic cavities

Bias magnetic field is especially non-uniform in the first block of the tuner - the one closest to the accelerating gap in Fig. 1; the distribution of the time-averaged density of the RF power loss in this block is also expected to be non-uniform. Map in Fig. 3 illustrates the degree of the non-uniformity of the power loss density distribution of the in the top part of the first block of the tuner.

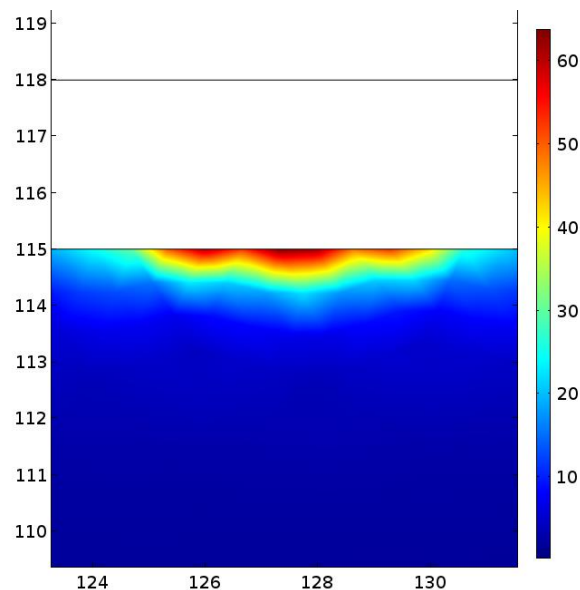


Fig. 3. RF loss power density distribution in the top block at 75 MHz (relative units).

As the resonance frequency of the cavity changes driven by the changing bias magnetic field, the distribution of the power loss also changes. Generally speaking, it is possible to find the average power density of the RF loss in each point of the tuner by making multi-physics modeling in the time domain. As this way is prohibitively time-consuming, another approach was suggested in [2]: to deal with the non-uniformity of the RF loss power density, the first block of the tuner was subdivided into several areas (smaller where the highest non-uniformity was observed), the space-averaged power loss was found in each area, it was then expressed as a function of the frequency and integrated over the required frequency range to find space- and time-averaged RF power loss density. Map in Fig. 4 shows this averaged power density in the first block of the tuner and in the ceramic disks at the top and at the bottom. Summing time-averaged RF loss power in all partial areas of this block gives the total RF power loss in the first block: **P1 = 436 W**.

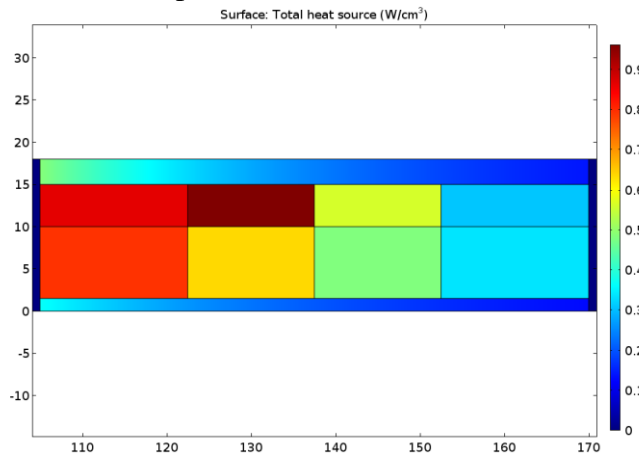


Fig. 4. Time- and space-averaged RF power loss density in the first block (W/cm^3).

Resulting temperature field in the blocks depends on the quality of their thermal contact with the heat sinks. Perfect thermal contact between the ferrite block and ceramic discs is assumed at this time as the surfaces of both parts can be made flat to the microns. Let's also assume using thermally conducting filler between the inner and outer cylindrical surfaces of the blocks and the heat sink (constant temperature boundary) and an insulating condition between the inner and outer cylindrical surfaces of the ceramic disks and the heat sinks. These assumptions reflect possible loss of the contact between the disks and the sinks due to the difference in the thermal expansion coefficients of the materials in the tuner. Corresponding temperature map is shown in Fig. 5: temperature rise relative to the temperature of the heat sink is shown in the figure.

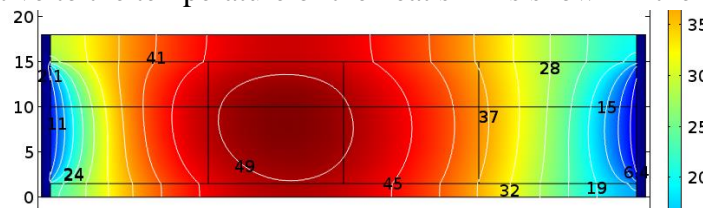


Fig. 5. Temperature rise in the top (1-st) disk of the RF tuner (in Celsius).

The maximum temperature rise of $\sim 50^{\circ}C$ is observed in the center of the block, not where the maximum power density was in Fig. 3. This can be considered as needed assurance that (1) the disks introduced to help with the heat removal do work as desired, and (2) that possible run-away situation at the spots with the maximum static heat load can be avoided.

The results obtained in [2] are encouraging, but the addition of the second block to the model resulted in some unwanted (and rather unexpected) sequences. First, the maximum temperature in the second block was now higher than in the first one in spite of the fact that the RF loss power density was higher in the first block. Increased thickness of the block (22 mm) is the reason here. Higher temperature of the second block generates thermal flux into the first block that elevates its temperature (Fig. 6). The maximum temperature rise in the first block is now 52.5°C. The maximum temperature rise in the second block is ~56°C.

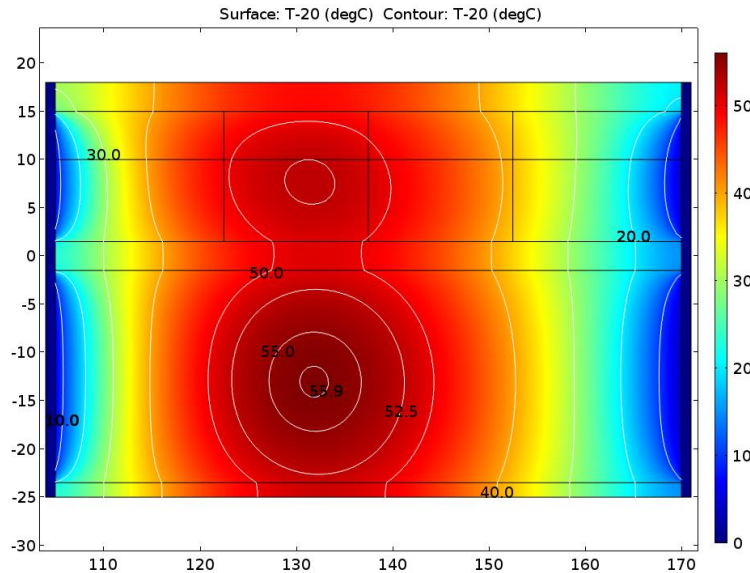


Fig. 6. Temperature rise in the two top blocks of the RF tuner (in Celsius).

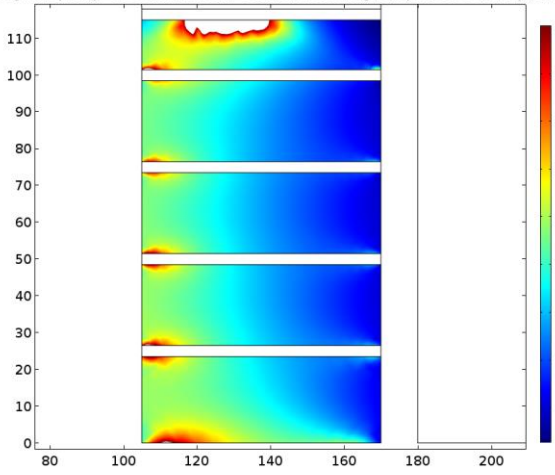
The increase of the maximum temperature in the block that is closer to the middle area of the tuner triggered the need of a study that would take into account the whole tuner, not just a part of it. The main goal of the study is to make sure we grasp the thermal situation for the whole system. Potential benefit of this exercise is that the thicknesses of the blocks can be re-optimized to cap the temperature rise.

Following the pattern developed in [2], first thing we need to find is analytical approximation for the RF loss power density spatial distribution in the rest of the blocks of the tuner stack.

RF loss distribution in the central blocks (#2, #3, and #4) of the tuner

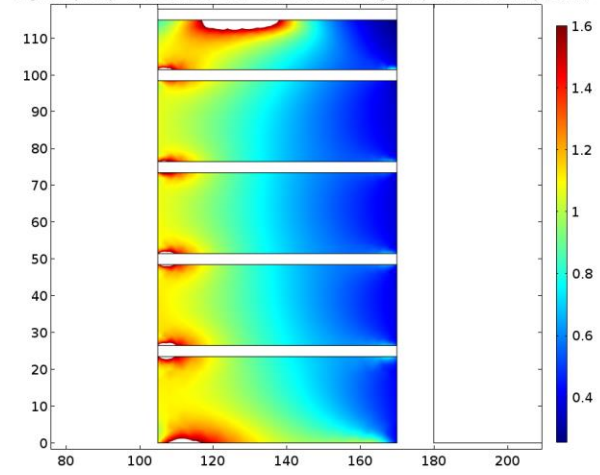
Figures shown below map the RF loss power density in all blocks of the tuner at frequencies corresponding to several settings of the bias current. One can see that the spatial distribution of the RF loss power density in the three middle blocks of the tuner depends mostly on the radius, and only weakly on the axial coordinate. In these figures, the power conversion coefficients k_W must be applied at each current setting to get the values of the power density corresponding to the required 100 kV accelerating voltage. For example, for the figure corresponding to the bias current of 6.5 kA, coefficient $k_W = 9.172 \cdot 10^6$, and the scaling results in the maximum power loss density $\sim 17 \text{ W/cm}^3$; the minimum will be $\sim 3 \text{ W/cm}^3$. Table 1 that follows this set of figures summarizes the results of the total static (that is corresponding to a particular current setting) RF loss power calculation for each block and disk in the tuner (in Watts).

Eigenfrequency= $7.3934E7+14684i$ Surface: Electromagnetic power loss density (W/m^3)



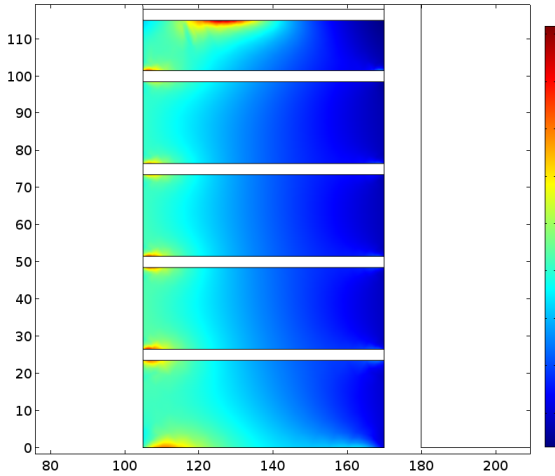
Iw = 6.5 kA

Eigenfrequency= $7.7201E7+12742i$ Surface: Electromagnetic power loss density (W/m^3)



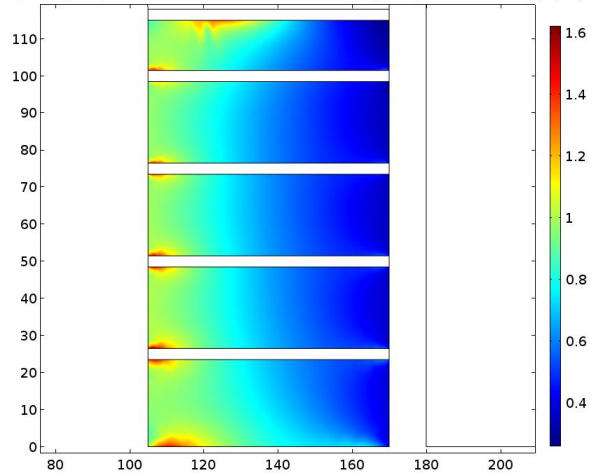
Iw = 7.0 kA

Eigenfrequency= $7.999E7+11453i$ Surface: Electromagnetic power loss density (W/m^3)



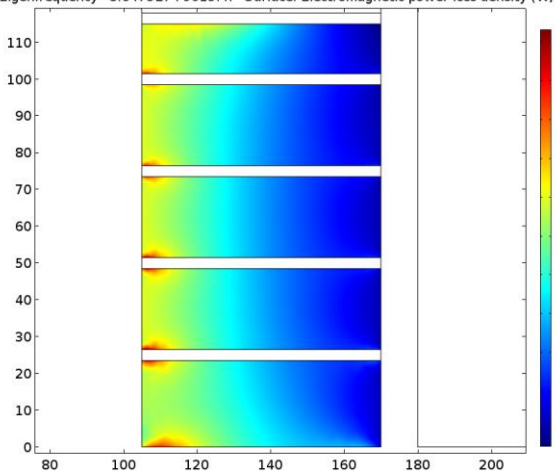
Iw = 7.5 kA

Eigenfrequency= $8.2419E7+10468i$ Surface: Electromagnetic power loss density (W/m^3)



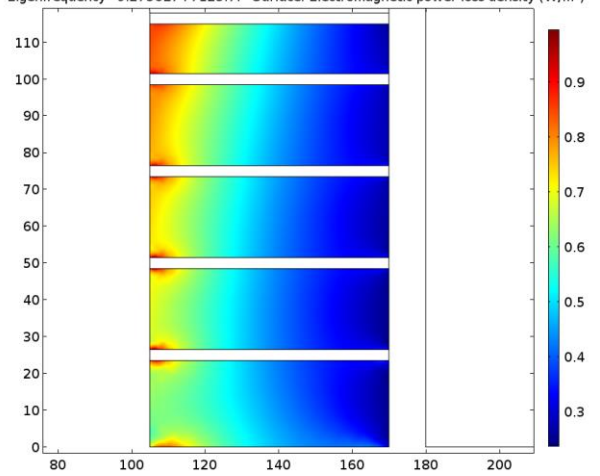
Iw = 8 kA

Eigenfrequency= $8.6475E7+9015.4i$ Surface: Electromagnetic power loss density (W/m^3)



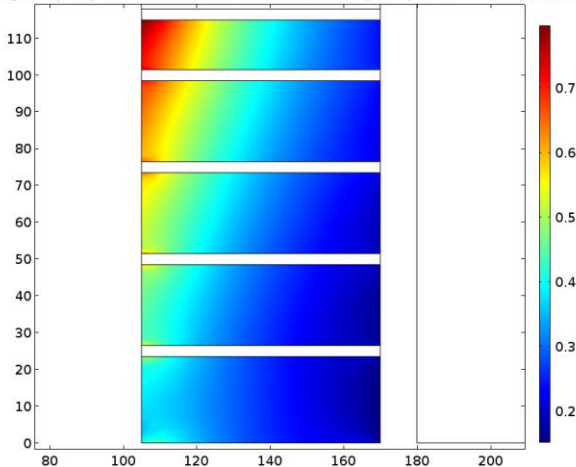
Iw = 9 kA

Eigenfrequency= $9.2736E7+7123.7i$ Surface: Electromagnetic power loss density (W/m^3)



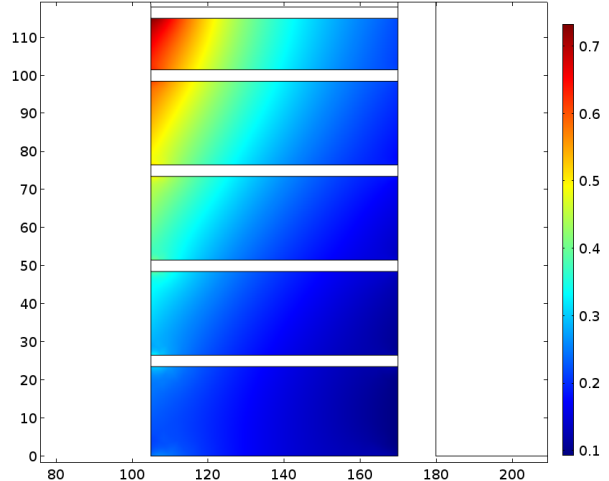
Iw = 11 kA

Eigenfrequency=1.0095E8+5134.9i Surface: Electromagnetic power loss density (W/m³)



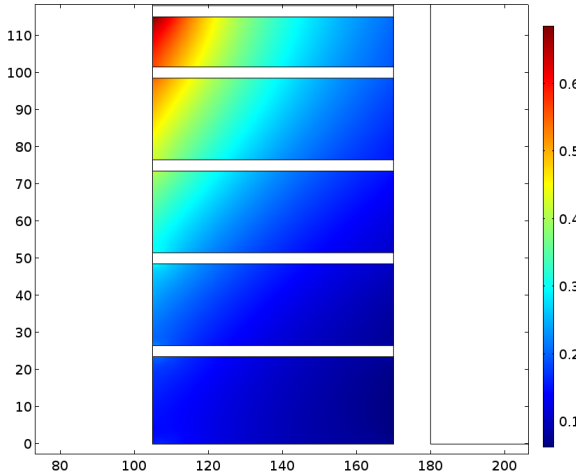
Iw = 15 kA

Eigenfrequency=1.0671E8+4036.4i Surface: Electromagnetic power loss density (W/m³)



Iw = 20 kA

Eigenfrequency=1.1043E8+3448.3i Surface: Electromagnetic power loss density (W/m³)



Iw = 25 kA:

Table 1. Static RF power loss in the blocks of the tuner

Iw (kA)	6.5	7.0	7.5	8	9	11	15	20	25
f (MHz)	73.93	77.20	79.99	82.42	86.49	92.74	100.95	106.71	110.43
k _w · 10 ⁻⁶	9.172	8.995	8.838	8.699	8.460	8.080	7.577	7.226	7.001
D1 (W)	453	447	440	433	418	389	342.5	305	280
B1 (W)	7919	6001	5093	4519	3618	3091	2405	2004	1771
D2 (W)	355	358	357	355	347	326	288	257	235
B2 (W)	8565	7846	7191	6663	5604	4800	3524	2804	2394
D3 (W)	227	230.5	232	231.5	228	214	190	170	155
B3 (W)	8589	7925	7336	6811	5658	4568	3053	2207	1757
D4 (W)	113.5	115.9	116.7	116.5	115	108	95.5	84.8	110
B4 (W)	9089	8384	7728	7117	5794	4408	2657	1699	1218
D5 (W)	32.5	33	33	33	32	30	26.4	23.2	22
B5 (W)	11236	10155	9174	8313	6584	4808	2635	1512	966
ΣD (W)	1181	1185	1179	1169	1140	1067	942	840	802
ΣB (W)	45398	40311	36522	33423	27258	21675	14274	10226	8016
ΣP (W)	46579	41496	37701	34592	28398	22742	15216	11066	8818

In Table 1, for each bias current I_w , resonance frequency of the cavity and the power conversion coefficient k_w are found. Static RF power loss is calculated for each block (B1 to B5) and each ceramic disk (D1 to D5). The bottom disk was not taken into account as the power loss in this disk is of pure electrical nature, and the electric RF field is near zero at the location of this disk. Last three rows in the table sum the powers in the discs (ΣD), in the blocks (ΣD), and in the whole tuner (ΣP). Total dissipated power in the tuner ΣP agrees with what was found in [2].

For each block of the tuner, a series of graphs are extracted that show how the RF loss power density changes in space. As an example, **for the 2-nd block** and with the $I_w = 6.5$ kA bias, the power density values along the three radial lines - at the top, at the center, and at the bottom of the block - are plotted in Fig. 7. As earlier, the power conversion coefficient $k_w = 9.17 \cdot 10^6$ must be used to get the numbers corresponding to 100 kV accelerating voltage.

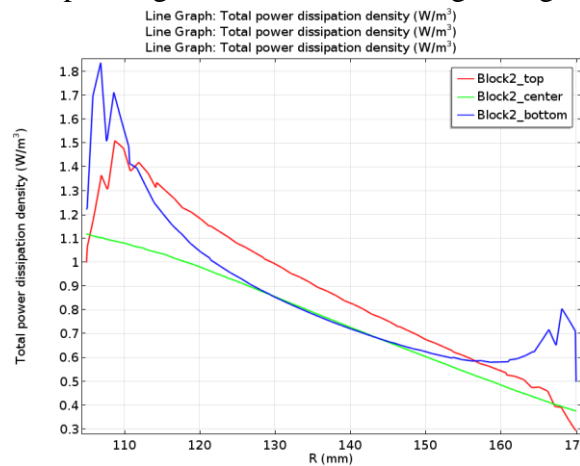


Fig. 7. RF loss power density in the second block of the tuner at $I_w = 6.5$ kA

In this block (block #2), for every setting of the current, we will assume linear drop of the loss power density with the radius:

$$p(r, I_w) = p(r_{in}, I_w) - dp/dr(I_w) \cdot (r - r_{in}) \quad /1/$$

Coefficients to use with this expression at each current setting are found by calculating the total power loss in the block using /1/ and comparing results with those in Table 1. Table 2 provides the values of the coefficients found this way with $r_{in} = 11$ cm.

Table 2. Coefficients in the expression /1/ as function of the bias current (block #2)

I (kA)	$p(r_{in})$ (W/cm ³)	dp/dr (W/cm ⁴)
6.5	11	1.3
7.0	10	1.17
7.5	9.3	1.06
8.0	8.5	0.97
9	7.28	0.81
11	6.06	0.68
15	4.5	0.5
20	3.6	0.4
25	3	0.32

Dependence of the parameters on the current can be approximated by the following expressions (current in kA, the dimensions in cm, and the power density in W/cm³):

$$p_{in_appr} = 50/(Iw-1)^{0.9} \tag{2/}$$

$$dp/dr_{appr} = 4.2/(Iw-2.5)^{0.85} \tag{3/}$$

Graphs below compare the coefficients calculated using the approximation /2/ and /3/ (red line) with those in Table 2 (circles).

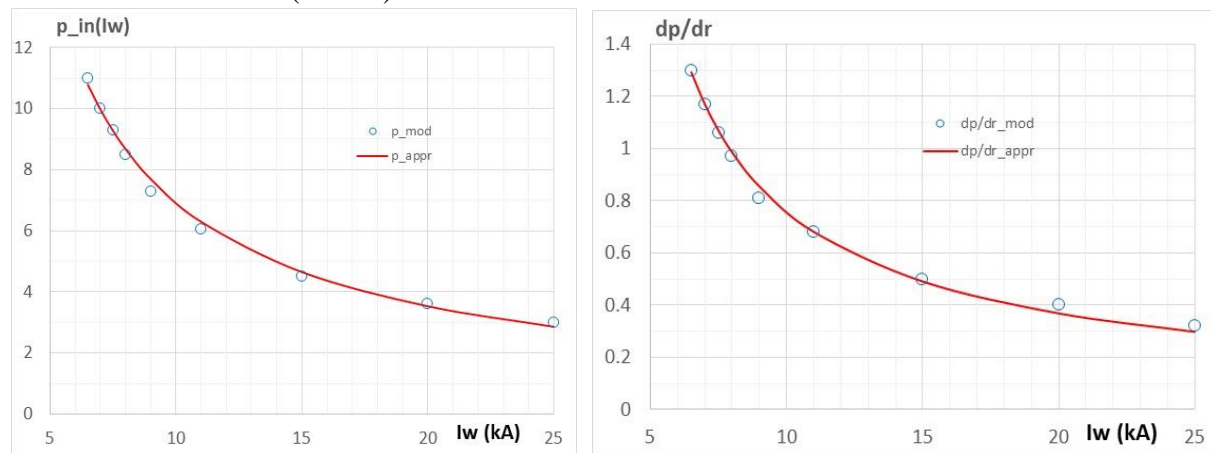


Fig. 8. Calculated (circles) and approximated (red line) coefficients in expression /1/ as functions of the bias current

As a result, expression /1/ for the static RF power loss **in the second block** can be re-written as a function of the radius and the current:

$$p(r, Iw) = 50 \cdot (Iw-1)^{-0.9} - 4.2 \cdot (Iw-2.5)^{-0.85} \cdot (r-11) \tag{4/}$$

By formally integrating /4/ over the volume of the block, we can find the total dissipated power at different bias currents. Results can be compared with what was found for each bias setting by assuming the linear dependence on the radius with the coefficients posted in Table 2 and with losses posted in Table 1, where no special assumptions on the power density spatial distribution were made.

Table 3. RF loss power (W) in the second block found using different approaches

Iw (kA)	Using /4/	Table 2	Table 1
6.5	8513	8800	8565
7.0	7968	8009	7850
7.5	7484	7553	7191
8.0	7054	6910	6663
9.0	6325	5983	5604
11.0	5244	4960	4800
15.0	3920	3700	3520
20.0	2993	2962	2804
25.0	2430	2517	2394

For every setting of the current (except 6.5 kA), the values of power loss in the second block found using expression /4/ are slightly higher than that found without making any special assumption about the RF loss power density distribution; this provides some reserve.

Now we can apply the time averaging procedure developed in [2]. We will use the same function for the required frequency change in time:

$$\text{For } 0 < t < 3 \text{ ms} \quad f(\text{MHz}) = 75.7316 - 0.0466 \cdot t + 0.7774 \cdot t^2 - 0.0513 \cdot t^3 \quad /5a/$$

$$\text{For } 3 \text{ ms} < t < 25 \text{ ms} \quad f(\text{MHz}) = 65.3 + 6.47 \cdot t - 0.415 \cdot t^2 + 0.0128 \cdot t^3 - 0.00018 \cdot t^4 + 8.3 \cdot 10^{-7} \cdot t^5 \quad /5b/$$

and for the bias current dependence on the frequency

$$Iw(f) = 5.2 + 0.135 \cdot (f-65) + 0.002 \cdot (f-65)^2 - 1.1 \cdot 10^{-4} \cdot (f-65)^3 + 4.6 \cdot 10^{-6} \cdot (f-65)^4. \quad /6/$$

As in [2], the 100 kV RF accelerating voltage is applied only in the intervals $0 < t < 3$ ms and 16 ms $< t < 19$ ms. As a result of the averaging, the following expression for the average RF loss power density in the block #2 can be written:

$$p \text{ (W/cm}^3) \approx 1.7 - 0.086 \cdot r \text{ (cm)} \quad /7/$$

The time-average power dissipated in the second block during the cycling with the 15 Hz repetition rate is found by integrating expression /7/ over the volume of the block: **P2 ≈ 613 W**.

One can see from figures on pages 5 and 6 of this note that distribution of the power loss density in blocks #2, #3, and #4 are quite similar except at the high current settings. To make the time and space averaging of the power loss in the blocks #3 and #4, a procedure similar to what was used for the second block can be applied; results are summarized by the following expression:

$$p \text{ (W/cm}^3) \approx 1.3 - 0.056 \cdot r \text{ (cm)} \quad /8/$$

The average power dissipated in the blocks #3 and #4 is found by integrating expression /8/ over the volume of the blocks: **P3 ≈ P4 ≈ 640 W**.

RF loss distribution in the bottom (5-th) block of the tuner

This block is the 23.5 mm thick, and it is located at the point where RF magnetic field in the cavity is the highest; so we can expect significant RF loss density in this block. As it was done earlier, the average power loss in this block can be evaluated by mapping the power loss density at several fixed bias currents followed by the time averaging procedure. As an example of the mapping, the RF loss power density distribution at 6.5 kA bias current is shown in Fig. 9.

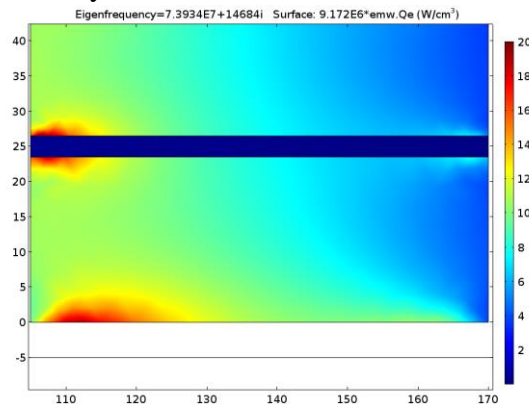


Fig. 9. RF loss power density in the bottom block at 6.5 kA bias current

The maximum heating power density in the block is $\sim 20 \text{ W/cm}^3$. As it was done earlier, distribution of the RF losses was visualized by graphs along several straight lines (radial and axial) in the block. Approximating expression was suggested that expanded this information through the volume of the block with coefficients that depend on the bias current:

$$p(r, z) = A \cdot [1 + B \cdot (z - 2.3)^2] \cdot [1 - C \cdot (r - 11)] \tag{9/}$$

As earlier, in this expression r and z are in centimeters, and p is in W/cm^3 .

For each current setting, coefficients A, B, and C were found that provide acceptable fit for the data obtained by modeling. A set of the coefficient values obtained that way was expressed as an expansion functions of the current by using the following fits:

$$A = 445 \cdot (I_w + 2.5)^{-1.7} - 0.6 \tag{10a/}$$

$$B = 0.75 \cdot (I_w - 4)^{-1.7} \tag{10b/}$$

$$C = 0.1 \tag{10c/}$$

Table 4 compares the values of the coefficients A and B found for each current setting with those calculated using expressions /10/. Graphs in Fig. 10 visualize Table 4: coefficients A and B found for each current setting (squares) are compared with those found by using the fitting expressions /10/ (red line).

Table 4. Coefficients in the fitting expression /9/ for different bias currents

I _w (kA)	6.5	7	7.5	8	9	11	15	20	25
A_model	10	9.2	8.5	8	7	5.2	2.9	1.6	1.1
A_fit	10.021	9.088	8.279	7.572	6.401	4.731	2.829	1.637	0.990
B_model	0.15	0.12	0.1	0.08	0.05	0.025	0.01	0.005	0.001
B_fit	0.1580	0.1159	0.0892	0.0710	0.0486	0.0274	0.0127	0.0067	0.0042

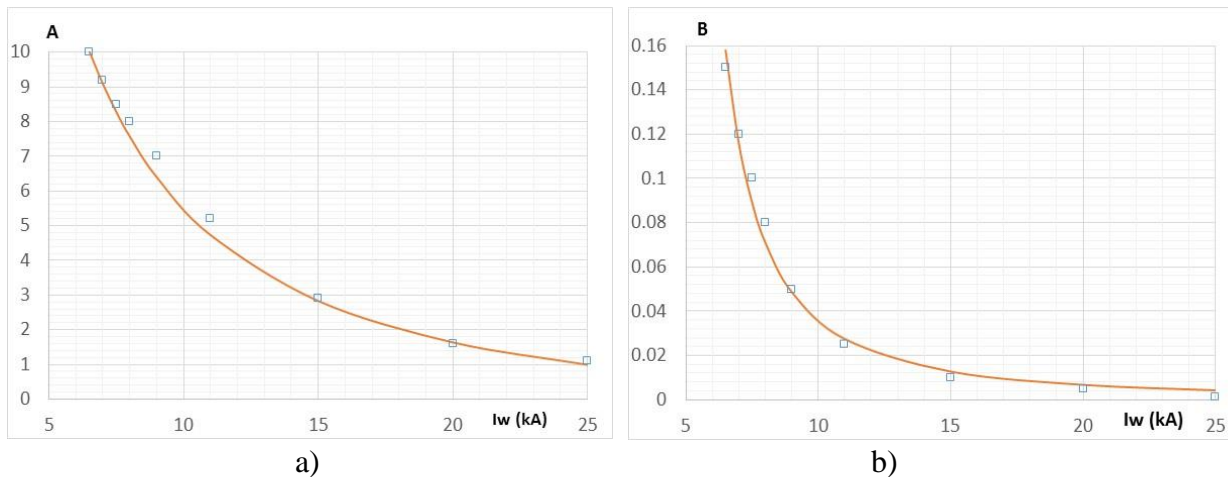


Fig. 10. Coefficients A (a) and B (b) of the expression /10/ as functions of the current.

At each current setting, the total RF loss power in the block can be found by integrating /9/ over the volume of the block; results of this operation are close to what was posted in Table 1.

The interpolating expression /9/ for the RF loss power density in the bottom block expresses it as a function of the position and the bias current. Nevertheless, unlike it was done in the case of

the second block, we cannot use the averaging procedures for the coefficients because for the bottom block we have a non-linear interpolating expression. Instead we will follow the way used when the study of the first block was made. Let's break the cross-section of the bottom block into several rectangular areas (small enough to neglect the nonlinearity within each area) and find values of the RF loss power density in the centers of each area. We will use these values to represent spatially averaged power density for each area. Centers of each area are at the crossing of the following lines in the cross-section:

$Z = 0.3 \text{ cm}$, $Z = 1.175 \text{ cm}$, $Z = 2.05 \text{ cm}$,

$R = 11 \text{ cm}$, $R = 12 \text{ cm}$, $R = 13 \text{ cm}$, $R = 14 \text{ cm}$, $R = 15 \text{ cm}$, $R = 16 \text{ cm}$, and $R = 17 \text{ cm}$.

The height of the areas at the bottom and at the top of the bottom block is 6 mm. The height of the areas in the center of the block is 11.5 mm. The widths of all areas, except the areas with the centers at $r = 17 \text{ cm}$, are 10 mm. The width of the areas with the centers at $r = 17 \text{ cm}$ are 5 mm.

Expressions /9/ with the coefficients defined by /10/ were used to find the time- and space-averaged values of the power density in each area. Table 5 shows the found values of the time and spatially averaged power density for each area (in W/cm^3).

Table 5. Time and spatially averaged power density for each area of the bottom block (W/cm^3)

R (cm)	11	12	13	14	15	16	17
Z = 0.3 cm	0.83	0.75	0.67	0.58	0.5	0.42	0.33
Z = 1.175 cm	0.68	0.62	0.55	0.48	0.41	0.34	0.27
Z = 2.05 cm	0.61	0.55	0.49	0.43	0.37	0.31	0.25

A map of the time and spatially averaged power density in the bottom block is shown in Fig. 11.

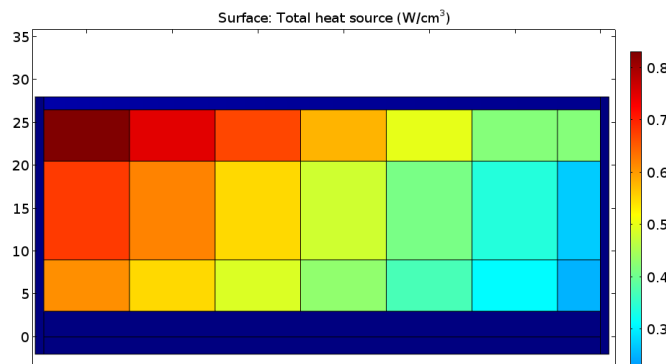


Fig. 11. A map of the time and spatially averaged power density in the bottom block.

Knowing the averaged power density for each area, it is straightforward to calculate the time-averaged RF loss power in the bottom block by summing the losses in all partial volumes defined by corresponding cross-sectional areas; the calculation results in the average RF loss power in the bottom block $P_{\text{bott}} = 650 \text{ W}$.

Power loss in the Alumina disks

Let's evaluate the RF loss power density in the alumina disks (loss tangent $\text{tg}(\delta) = 10^{-4}$) of the tuner. As the disks are relatively thin (3 mm) only one-dimensional spatial distribution will be used. For disks #1 and #2, we will use the function obtained in [2].

For the disk #1 (top):

$$p(r, Iw) = A(Iw)/r^{2.6} \quad [\text{W/cm}^3] \quad /11a/$$

$$A(Iw) = 2730 - 60 \cdot Iw \quad [\text{W/cm}^{0.4}] \quad /11b/$$

As before, in this expression r is in centimeters, Iw in kA, and p in W/cm^3 . Coefficient A in the expression is a linear function of the current, so it can be averaged in the active range of the frequencies (Fig. 2). After the 15 Hz repetition rate is taken into account, the following expressions for the time-averaged RF loss power density in disk #1 can be written:

$$p_{d1} (\text{W/cm}^3) = 220.5/r^{2.6} \quad /12/$$

Integration over the volume of the disk gives the total RF power loss here $P_{d1} \approx 42.5 \text{ W}$.

Similar expressions found in [2] for the second disk are

$$p(r, Iw) = A(Iw)/r^{2.2} \quad [\text{W/cm}^3] \quad /13a/$$

$$A(Iw) = 530 - 15 \cdot Iw \quad [\text{W/cm}^{0.8}] \quad /13b/$$

$$p_{d2} (\text{W/cm}^3) = 65/r^{2.2} \quad /14/$$

Integration over the volume of the disk #2 gives the total RF power loss $P_{d2} \approx 38 \text{ W}$.

The disk installed at the bottom of the bottom of the tuner (disk #6) has quite low losses as the electric field is close to zero.

RF power loss in the disk on the top of the bottom block (disk #5) can also be described as a linear function of the bias current, so the procedure used earlier in the studies of the first and the second blocks can be employed. For all bias current sets, radial distribution of the **static** RF loss power density can be described using the expression

$$p = A/r^{2.0} \quad /15a/$$

$$A(Iw) = 42.65 - 0.865 \cdot Iw \quad /15b/$$

Table 6 compares the values of the coefficient A found using expressions /15/ with what was evaluated based on the modeling. The last row in the table shows the total power generated in this disk at each current setting calculated using /12/; this data must be compared with similar data in Table 1 obtained from the model by direct integration.

Table 6. Calculated and interpolated coefficients in the expression /12/

Iw (kA)	7	8	11	15	20	25
A_model	37	36	33	29	25	22
A_calc	36.6	35.7	33.1	29.7	25.3	21
P (W)	33.2	33	30	26	22.5	21.5

The time averaging procedure applied to the coefficient A in /15/ results in the following expression for the average RF loss power density (in W/cm^3) in the disk #5 on the top of the bottom block:

$$p_{d5} = 3.75/r^2 \quad /16/$$

Total RF power dissipated in this disk $P_{d5} = 3.5 \text{ W}$.

The average RF loss power density in the disks #3 and #4 is found using the same approach: for the disk #3

$$p_{d3} = 33/r^2 \quad /17/$$

with the total RF power $P_{d3} \approx 30 \text{ W}$, and for the disk #4

$$p_{d4} = 20/r^2 \quad /18/$$

with the total RF power $P_{d4} = 18 \text{ W}$.

Now we have all information needed to set thermal problem for the tuner. Fig. 12 shows a map of the average power density distribution in the ferrite material of the tuner and in the ceramic disks.

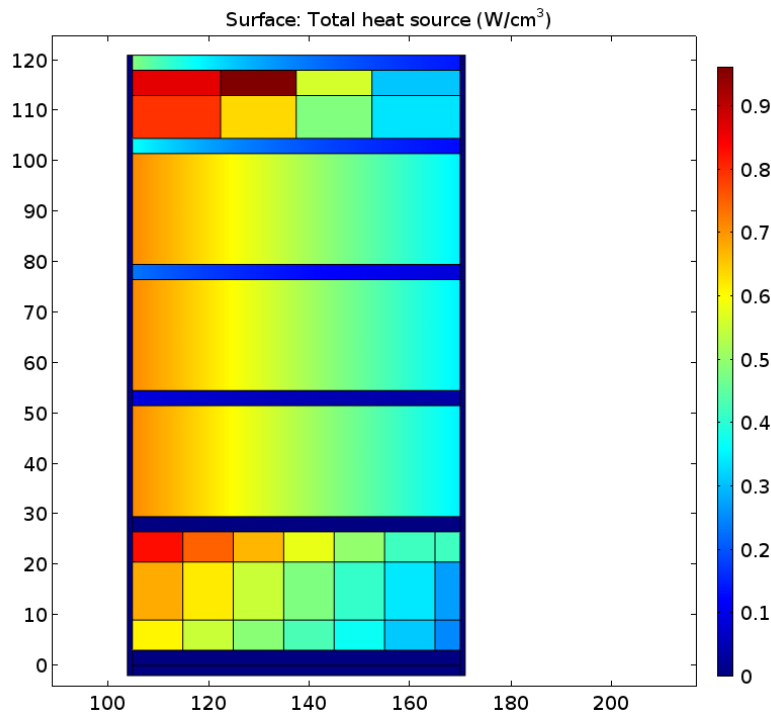


Fig. 12. A map of the time and spatially averaged power density in the tuner

First, as in [2], let's consider the case when thermal contact of the ferrite block to the water-cooled body of the cavity is made using a 0.25 mm thick thermal paste ($k = 1 \text{ W/(m}\cdot\text{K)}$) and the alumina disks do not have any thermal contact with the body of the cavity. They have a **perfect** thermal contact to the garnet blocks though; this contact helps in removing the heat from the central part of the blocks bypassing the thick low-conducting part of the garnet blocks. Temperature rise map of the tuner that we got using these assumptions is shown in Fig. 13. The maximum temperature rise inside the central blocks is $\sim 55^\circ\text{C}$. Assuming the cooling water temperature of $\sim 40^\circ\text{C}$, we get the maximum temperature inside the blocks of $\sim 95^\circ\text{C}$, which still can be tolerated for this type of the ferrite material.

One of the problems that can be expected is non-uniform bulging of the blocks due to the temperature expansion; the only way to minimize the non-uniform bulging is to limit the temperature rise by optimizing thicknesses of the blocks.

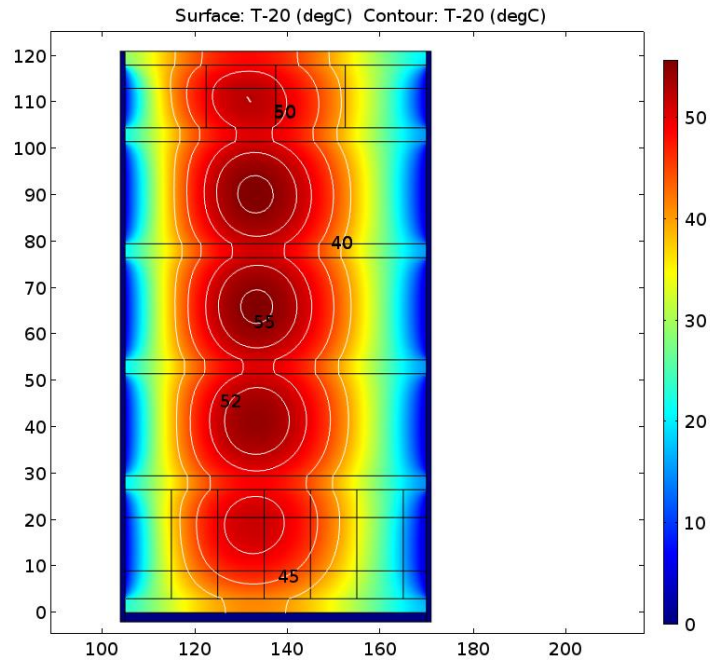


Fig. 13. A map of the temperature rise inside the tuner with good thermal contact along the peripheral parts of the garnet blocks.

To understand how critical is to have a good thermal contact between the garnet blocks and the cooled body of the cavity, let's assume good thermal contact along the outer surfaces of the alumina disks and make the blocks thermally insulated. Result is shown in Fig. 14; the maximum temperature rise becomes unacceptably high – 82.5°C.

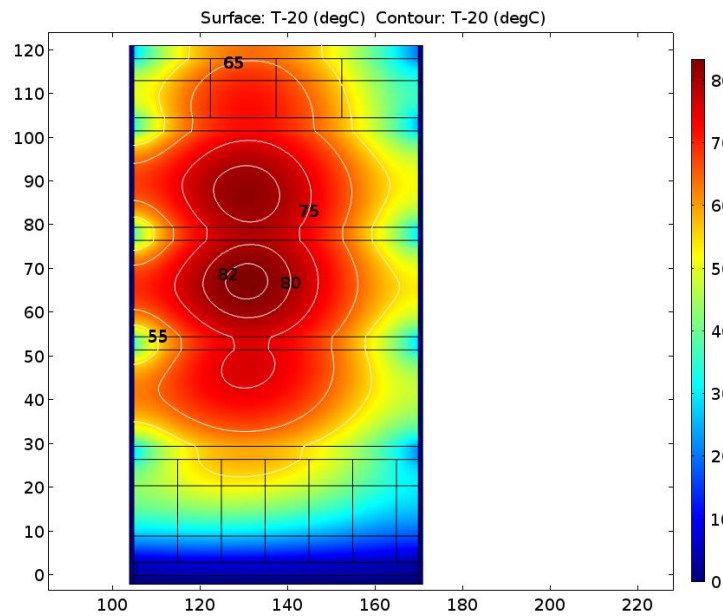


Fig. 14. A map of the temperature rise inside the tuner with good thermal contact along the peripheral parts of the alumina disks.

For verification purposes and to set requirements for cooling the surfaces of the cavity, let's find the heat fluxes that cross the boundaries of the ferrite blocks on the way to the heat sinks. Table 7 summarizes this information for each element of the tuner and compares the heat fluxes with the RF heat deposition.

Table 7. Heat flux balance table

	P_inner (W)	P_outer (W)	Total Flux (W)	P _{RF} (W)
D1	7.8	8.5	16.3	42
B1	226.5	239.5	466	436
D2	13.8	15.3	29.1	38
B2	299	308.5	607.5	613
D3	13.3	15.3	28.6	30
B3	289	324	613	637
D4	13	15.5	28.5	18
B4	284	321	605	637
D5	12	14	26	4
B5	297	329	626	651
D6	4.5	6.4	11	0
ΣP	1460	1598	3058	3090

Amount of the heat leaving the garnet material though the boundaries is well compared with what is generated inside; this is indication that the heat balance condition is observed.

Although thermal conductivity of the filler between the disks and the heat sinks is made 1000 times smaller than between the blocks and the sinks, still significant flux makes it through this boundary. This happens because higher conductivity of alumina results in more uniform temperature in the disks and higher gradients of the temperature at the boundary. Efforts must be applied to ensure that thermal contact between the blocks and the heat sink is not lost when the temperature rises during operation.

Tuner assembly procedure can make significant impact on the thermal boundary conditions. One of proposed ways to assemble the tuner is using pre-assembled elements consisting of glued together one garnet block and one alumina disk (0.1 mm thick layer with $k = 1 \text{ W}/(\text{m}\cdot\text{K})$). Expected advantage of this way is a possibility to precisely machine the assembly and thus avoid thermal discontinuity between the inner and outer cylinder surfaces of the disks and the heat sink. To provide some flexibility, these elements can be assembled in the tuner without using glue: pure mechanical contact or thermally conducting paste can be used instead between the elements. To understand feasibility of this approach, a model was run for the cases where the 0.25 mm thickness of thermal paste layers and 10 μm air gap between the elements were accepted.

For the case when no thermal contact was assumed between the disks and the heat sink, the maximum temperature rise of 57°C was observed in the second block (Fig. 13 shows the temperature rise 55°C with perfect axial thermal contact). When thermal contact of the disks was made corresponding to that of the block, the maximum temperature rise of 50°C was observed in the second and the third blocks (Fig. 15).

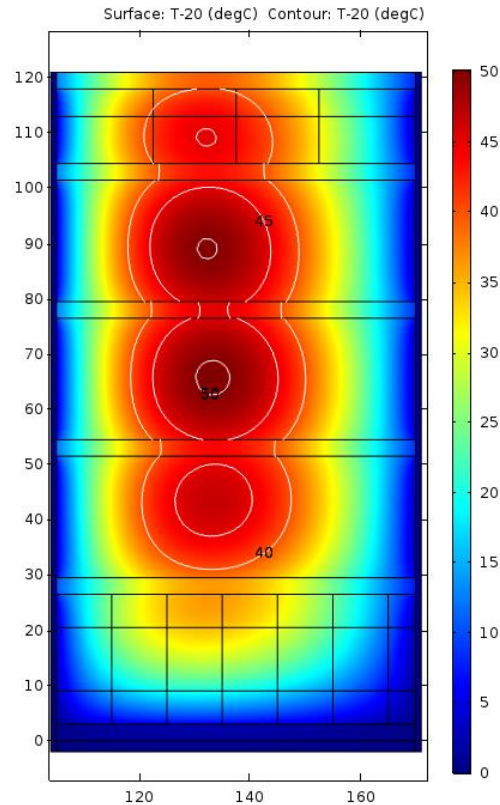


Fig. 15. A map of the temperature rise inside the tuner with 0.25 mm thermal paste between the peripheral parts of the garnet blocks and the alumina disks and thermal sinks and with 10 μm axial air gaps between the elements of the tuner assembly.

Conclusion

A study was made to evaluate the temperature rise inside the tuner of a tunable 2-nd harmonic booster cavity. It has been shown that the temperature rise is within the acceptable range for the AL-800 material.

Further optimization can be made to make the temperature lower and more uniform along the length of the tuner.

Design of the tuner must ensure good thermal contact between the garnet blocks and the cavity wall. Good thermal contact also between the disks and the walls will further improve thermal situation.

Bulging of the blocks and disks due to the non-uniform temperature field can lead to partial loss of the axial thermal contact between the blocks and disks.

References:

1. D. M. Poser, Microwave Engineering, John Wiley & Sons, Inc., 1998.
2. I. Terechkine, G. Romanov, "Thermal Analysis of the Tuner of the FNAL Booster's 2-nd Harmonic Cavity", FNAL TD note TD-15-020, Oct. 2015.